Modeling the Cycles of Growth and Detachment of Bubbles in Carbonated Beverages

Sébastien Uzel, Michael A. Chappell, and Stephen J. Payne*

Department of Engineering Science, University of Oxford, Parks Road, Oxford OX1 3PJ, U.K.

Received: November 11, 2005; In Final Form: February 9, 2006

In this paper, a model for the formation of bubbles in carbonated beverages is presented. It has previously been shown that bubbles form from cellulose fibers within such beverages and the passage of such bubbles from the fibers to the liquid surface has been modeled. A model is thus presented here that considers the process of formation, which is governed by diffusion through the fiber and bubble surfaces. The model comprises two stages, growth and detachment, and it is shown here that both play an important role. The latter process is found to occur over a much shorter time scale than the former, enabling the models to be partially decoupled. The total number of bubbles released from individual fibers over time is found to be approximated well by an exponential relationship, and the parameters in this relationship are presented for a range of different detachment angles and fiber sizes. It is found that bubble formation is promoted in narrow, long tubes, but that the time constant is solely determined by the rate of diffusion across the liquid surface. The surface tension is found to have minimal influence on the number of bubbles produced.

1. Introduction

Bubbles are found in an enormous variety of physical situations, from the common boiling of water in a pot to the more complex phenomenon of decompression sickness in divers. However, the formation of bubbles in all of these situations are determined by only four types of nucleation, depending upon the concentration of the gas in the liquid, or more precisely, the supersaturation ratio S [1]

$$S = \frac{X_L}{X_0} - 1 \tag{1}$$

where X_L is the mole fraction in the supersaturated liquid and X_0 is the equilibrium mole fraction. One of these types of nucleation, technically referred to as type IV nucleation or nonclassical heterogeneous bubble formation, occurs when bubbles are formed in preexisting gas pockets and is characterized by a relatively low supersaturation ratio (<10) and a spontaneous growth of the bubble.[2]

It was recently found that the nucleation sites in carbonated beverages are of this type.[3] Here, the nucleation sites are small particles of dust present in the atmosphere or left by the washing and drying processes. The dust particles have approximately the shape of cylindrical tubes, as shown in Figure 1.[4]

Once the liquid is poured into the container, pockets of air are trapped in the cavities within the fiber called lumens. As the dissolved gas tension in the carbonated beverage is some six times greater than the pressure inside the tube, the dissolved gas can diffuse through the permeable cellulose wall, generating a bubble stream.

In his studies, Liger-Belair essentially examined, by means of high-speed high-resolution photographs, the birth of the bubbles, their rise to the top of the containing vessel, and their bursting.[3,4] However, he did not consider the actual formation process of the bubble. In this paper, we thus add the missing step, i.e., the growth and detachment of the bubbles inside and out from the lumen. To do this, we have developed a mathematical model which simulates the formation of bubbles, right from the pouring of the beverage until the carbon dioxide supply is exhausted.

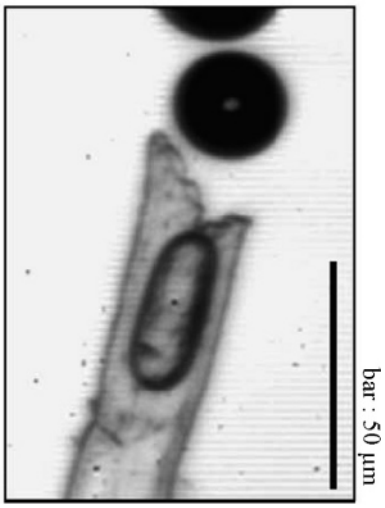

Figure 1. Photograph of a cellulose fiber releasing bubbles.[4]

This model is in fact very similar to and inspired by a physiological model of the formation of bubbles in the bloodstream of divers under decompression. Our previous work has examined the behavior of gas pockets trapped in crevices on vessel walls.[5] The two models are shown to exhibit very similar types of behavior, illustrating how the body can be considered to be like a large fizzy drink under decompression.

2. Materials and Methods

The model proposed here is thus based on the mathematical model for the growth of a bubble in a spherically symmetric crevice.[5] However, the geometry of the bubble growth in the cellulose fibers described above is different from this model,

* Corresponding author: e-mail, stephen.payne@eng.ox.ac.uk; tel, +44 1865 283306; fax, +44 1865 273905.

10.1021/jp056531x CCC: $33.50
Published on Web 03/21/2006

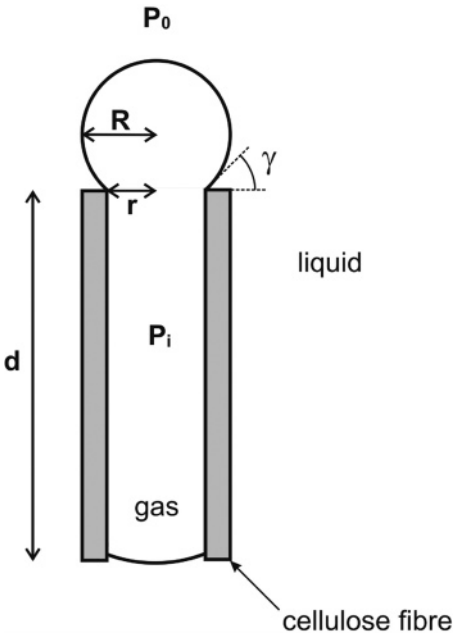

Figure 2. Definition of the tube geometry.

and the equations are thus slightly adapted. The cylindrical geometry considered here is shown in Figure 2. The proposed model is also different from that presented previously in that gas diffusion occurs through both the wall of the tube and the gas−liquid interface. In addition, only one gas needs to be considered (CO_2), rather than the multiple gases found in the body and considered by ref 5. The governing equations are outlined before the results from numerical simulations are presented in the next section.

A. Gas Transfer between Liquid and Bubble. Diffusion of gas within the liquid is described by the diffusion equation

$$\frac{\partial c}{\partial t} = D\nabla^2 c \tag{2}$$

where c is the concentration of gas (mol m^{-3}) and D is the bulk diffusion constant of the gas in the liquid (m^2 s^{-1}). Additionally we assume that changes in concentration are very rapid so that a quasi-static approximation can be made,[6] i.e., $\partial c/\partial t \approx 0$.

The rate of change of mass of gas in the bubble must equal the flux of gas through the bubble boundary, as described by the Fick equation

$$\frac{1}{\mathbb{R}T}\frac{\mathrm{d}}{\mathrm{d}t}(P_i V) = (A_0 D_0 + A_\perp D_\perp)\frac{\mathrm{d}c}{\mathrm{d}z}\Big|_{z=0} \tag{3}$$

where P_i is the pressure in the bubble (N m^{-2}), V is the total volume (m^3), T is the temperature (K), $\mathbb{R}$ is the specific gas constant, z is the radial distance (m), A_0 and $A_\perp$ are the surface area of the spherical cap of the bubble and the surface area of the lumen walls (m^2), respectively, and D_0 and $D_\perp$ are the bulk diffusion constants through those surfaces (m^2 s^{-1}). Temperature is assumed to remain constant at 20 °C.

Incorporating the one-dimensional solution to the diffusion equation gives

$$\frac{\mathrm{d}}{\mathrm{d}t}(P_i V) = L\left(\frac{D_0 A_0}{\lambda_0} + \frac{D_\perp A_\perp}{\lambda_\perp}\right)(P_t - P_i) \tag{4}$$

where P_t is the gas tension, equivalent to partial pressure (N m^{-2}), λ_0 and $\lambda_\perp$ are representative diffusion length scales (m), and L is the Ostwald coefficient for solubility, which has units of "gas volume, measured at ambient temperature and at 1 bar partial pressure, which dissolves in a unit volume of fluid" and whose value can be determined by the relation $L = 1413e^{a+bT^{-1}+c(\ln T)+dT}$, the parameters taken from ref 7.

It has further been shown that the diffusion length scales are very similar, hence $\lambda_0 = \lambda_\perp = \lambda$, and that $D_\perp$ and D_0 are approximately linked by the relation $D_\perp = 0.2D_0$.[4] The fiber wall is permeable, as shown by ref 8, which has a very significant impact on the behavior of the model. Thus

$$\frac{\mathrm{d}}{\mathrm{d}t}(P_i V) = LD_0\frac{(P_t - P_i)}{\lambda}(A_0 + 0.2A_\perp) \tag{5}$$

B. Gas Transfer between Liquid and Atmosphere. Since we only consider a single bubble stream, the change of P_t is primarily due to diffusion through the liquid−air interface at the top surface of the liquid and the gas transfer from other bubble streams. This can be approximated by a first-order differential equation

$$\frac{\mathrm{d}P_t}{\mathrm{d}t} = \frac{P_{\mathrm{amb}} - P_t}{\tau} \tag{6}$$

The time constant is then approximately

$$\tau = \frac{h\lambda}{D_0} \tag{7}$$

where we consider a vessel of constant cross-sectional area and height h (m), since the release of gas by bubbling represents only 20% of the gas transfer[9] and the bubble streams are not all concurrent. The time constant, τ, is sometimes defined as the half-time of diffusion, τ log 2.

C. The Laplace Equation. The effect of surface tension at the gas−liquid interface is incorporated using the Laplace equation

$$P_i = P_{\mathrm{amb}} + \frac{2\sigma}{R} \tag{8}$$

where P_{amb} is the ambient pressure (N m^{-2}), σ is the gas−liquid interface surface tension (N m^{-1}), and R is the radius of curvature of the interface (m). Although this equation is strictly only true in the steady state, it has previously been shown that this equation provides an excellent approximation for the dynamic formation of bubbles in crevices.[5] In Appendix A, we show that this is also true here.

D. Lumen Geometry. Simple geometry for a lumen bubble with a spherical gas−liquid interface gives a volume

$$V_i = \pi r^2 d\left(1 + \frac{r}{d}\frac{\zeta}{3}\right) \tag{9}$$

where the geometrical parameters are defined in Figure 1 and

$$\zeta = \frac{2 + (2 + \sin^2\gamma)\cos\gamma}{\sin^3\gamma} \tag{10}$$

as in ref 10. The surface areas are calculated from

$$A_0 = 2\pi r^2\frac{(1 + \cos\gamma)}{\sin^2\gamma}$$
$$A_\perp = 2\pi r d \tag{11}$$

Finally, the radius of curvature, R, of the gas−liquid interface can be rewritten in terms of the interface angle, γ, and the radius of the tube, r, as

$$R = \frac{r}{\sin \gamma} \tag{12}$$

E. Bubble Growth. Unlike in Chappell and Payne,[5] the growth of the bubble inside the tube is not considered, as this only adds a delay in the formation of the first bubble. Since the number of bubbles produced here is large, this slight delay is of negligible importance. The simulations described below thus start with a full tube and a flat interface ($\gamma = 180°$).

The behavior of the phenomenon is described by a system of only two differential equations, describing the growth of the bubble outside the tube

$$\left.\begin{aligned} \frac{dP_i}{dt} &= \frac{\frac{2LD_0}{\lambda r}\xi(P_t - P_i) + \frac{1}{4}\frac{r}{d}P_i\frac{d\gamma}{dt}\operatorname{cosec}^4\left(\frac{\gamma}{2}\right)}{\epsilon} \\ \frac{d\gamma}{dt} &= \frac{\frac{2LD_0}{\lambda r}\xi(P_t - P_i) + \epsilon\frac{dP_{amb}}{dt}}{2\frac{\sigma\epsilon}{r}\cos\gamma - \frac{1}{4}\frac{r}{d}P_i\operatorname{cosec}^4\left(\frac{\gamma}{2}\right)} \end{aligned}\right\} \tag{13}$$

where

$$\xi = 0.2 + \frac{r}{d}\frac{1+\cos\gamma}{\sin^2\gamma} \tag{14}$$

$$\epsilon = 1 + \frac{r}{d}\frac{\zeta}{3} \tag{15}$$

We also define a diffusion time constant as $\tau_D = \lambda r/LD_0$.

Note that only diffusion through the lumen wall and the top spherical cap has been considered. The spherical cap on the other side of the tube has been omitted, due to its much smaller surface area. It is assumed here for simplicity that the tube is vertically orientated, so bubbles only form from the top surface.

F. Model of Detachment. Once the limit angle γ_s is reached, the bubble is pulled out of the mouth of the tube by several phenomena. The most obvious one is buoyancy, but observations have shown that this is not the only one.[11] The up thrust due to flow toward the surface of the bubble or aspiration due to any preceding bubbles should also be considered. However, since estimating this parameter is thus difficult, it is set as a variable and its influence on the model behavior is examined below.

Upon reaching γ_s, the bubble splits off to form a free bubble with a new meniscus being formed almost immediately, whose shape is determined by the return angle γ_r. To calculate this angle, we model this process of detachment in three steps. The first step represents the bubble once it has reached γ_s and is about to start rising up. The second one corresponds to the limit of splitting, just before a new meniscus is formed and a free bubble released, being the third step. These three steps are shown in Figure 3.

For simplicity, the detaching bubble is approximated by geometrical shapes. The region in which detachment occurs is modeled by two cones with the top part assumed to be a sphere. These two shapes are linked by ensuring that the surface is continuously differentiable. In addition, the distance between the bottom of the sphere and the detachment point is assumed to be the same as the height of the bottom cone. This assumption is found to be a reasonable one, based on experimental data from other studies, for example, Manasseh.[12] In this experiment, the bubbles were produced by passing air through a 4 mm nozzle submerged in water, the shape being measured 0.5 ms before

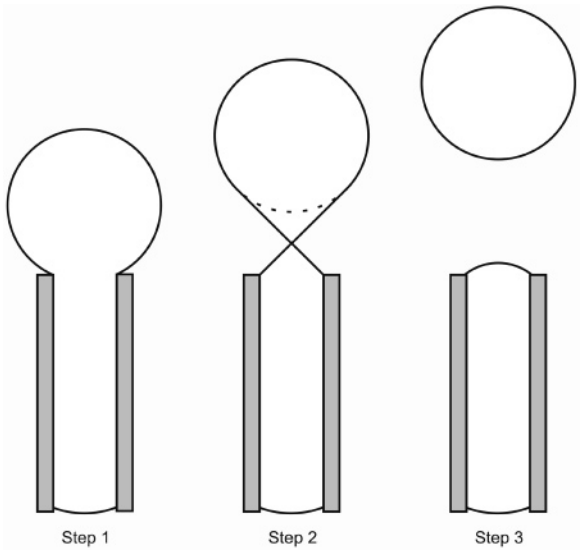

Figure 3. Description of the geometrical model of the bubble detachment.

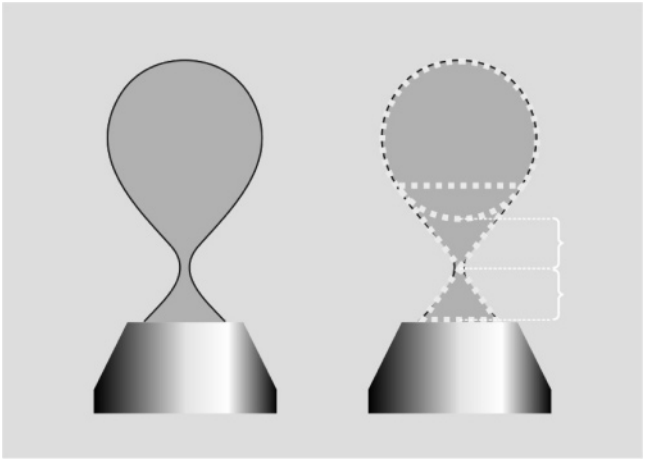

Figure 4. Approximate shape and geometrical best fit of a bubble at the limit of detachment, based on experimental data by Manasseh[12]

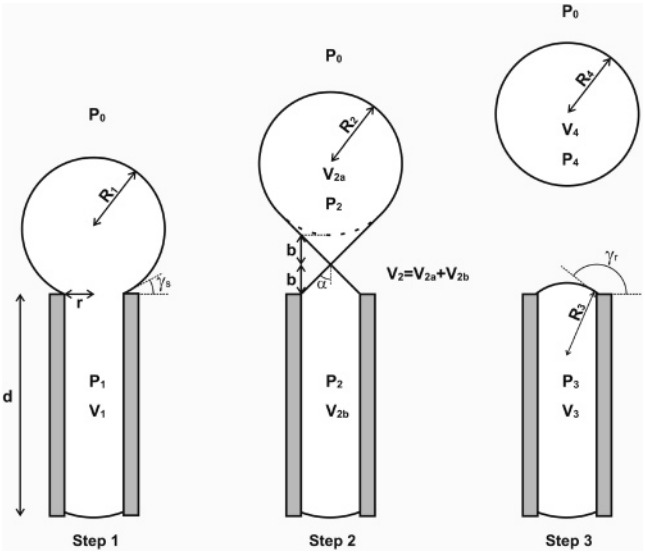

Figure 5. Definition of the parameters describing the three steps of detachment.

the breaking of the neck. The shape of the meniscus in this experiment is found to follow a simple geometrical shape, which we adopt here.

To determine the pressures, volumes, and radii of curvature at each step in the process, the Laplace equation is applied together with conservation of mass and geometrical considerations. It is assumed that this process occurs over a very short time period, such that diffusion plays a negligible role. The following set of equations whose parameters are detailed in Figure 5 can thus be derived.

Step 1:

$$P_1 = P_{amb} + \frac{2\sigma}{R_1}$$

$$V_1 = \pi r^2 d + \frac{\pi}{3} r^3 \frac{2 + (2 + \sin^2 \gamma_s) \cos \gamma_s}{\sin^3 \gamma_s}$$

$$R_1 = \frac{r}{\sin \gamma_s}$$

Step 2:

$$P_2 V_2 = P_1 V_1$$

$$P_2 = P_0 + \frac{2\sigma}{R_2}$$

$$V_2 = \pi r^2 d + \frac{\pi}{3} r^2 b + \frac{\pi}{3} R_2{}^2 (R_2 + b) \cos^4 \alpha + \frac{\pi}{3} R_2{}^3 \cos^3 \alpha \frac{2 + (2 + \cos^2 \alpha) \sin \alpha}{\cos^3 \alpha}$$

$$R_2 = \frac{b \sin \alpha}{1 - \sin \alpha}$$

$$\tan \alpha = \frac{r}{b}$$

Step 3:

$$P_3 V_3 = P_2 V_{2b}$$

$$P_3 = P_0 + \frac{2\sigma}{R_3}$$

$$V_3 = \pi r^2 d + \frac{\pi}{3} r^3 \frac{2 + (2 + \sin^2 \gamma_r) \cos \gamma_r}{\sin^3 \gamma_r}$$

$$R_3 = \frac{r}{\sin \gamma_r}$$

and

$$P_4 V_4 = P_2 V_{2a}$$

$$P_4 = P_0 + \frac{2\sigma}{R_4}$$

$$V_4 = \frac{4}{3} \pi R_4{}^3$$

For a given value of γ_s, the final pressure P_3 and the return angle γ_r can be directly calculated, together with the volume of the released bubble. This detachment model plays an important role as it provides the values of the change in pressure and angle during the detachment process. This joining together of the growth and detachment models is thus vital in modeling the cyclic pattern of bubble formation. The models can be solved in a largely decoupled manner, however, since the time scale for detachment is so much smaller than that for bubble growth. The bubble growth model thus provides the initial condition for the detachment model and vice versa.

TABLE 1: Governing Pseudonondimensional Parameters

governing parameter	dimensions	description
$\tau = h\lambda/D_0$	T	diffusion time constant across the top surface
$\tau_D = \lambda r/LD_0$	T	gas diffusion time constant
$\sigma' = \sigma/\bar{P}\bar{r}$		nondimensional surface tension
$r' = r/\bar{r}$		nondimensional tube radius
$d' = d/\bar{r}$		nondimensional tube length
γ_s		bubble detachment contact angle

TABLE 2: Physiological Parameters Used in the Model

parameter	value
T	20 °C
σ	0.0468 N m^{-1} [3]
L	0.997 mL of gas/mL of liquid[7]
D_0	1.4×10^{-9} m^2 s^{-1} [13]
h	10 cm
pseudonondimensional parameters:	
σ'	0.468
τ	1070 s
τ_D	107 ms

G. Model Parametrization. Similarly to the model of crevice bubbles,[5] the equations are recast into a pseudonondimensional form where only the time dimension is retained. The parameters $\bar{P}$ (1 bar) and $\bar{r}$ (1 μm) are introduced so that the equations can be rewritten in terms of nondimensional lengths and pressures. This improves the accuracy of the numerical solver and enables the nondimensional groups that govern the model behavior to be identified. In pseudonondimensional form, we thus identify six parameters which govern the dynamics of the lumen bubble. These parameters are given in Table 1, but to conserve space the equations are not reproduced in pseudonondimensional form here.

The particular beverage considered here is champagne, as many of the relevant model parameters have been measured, as given in Table 2. Default values for r, d, and γ_s are taken to be 10 μm, 100 μm, and 20°, respectively, although a range of values will be explored below. Those values are taken from photographs presented by refs 3 and 4, showing that there is a natural variation in these parameter values. The height h of the flute is set at 10 cm. The value of the parameter λ is estimated to be 15 μm,[4] and D_0 has been measured using MRI.[13] Finally, the value of σ was calculated using a pendant droplet apparatus.[3]

H. Estimating the Volume and the Pressure of Gas Liberated in Free Bubbles. The geometrical model cited before, as well as linking γ_s and γ_r, gives us further information, such as the pressure and the volume of the gas liberated in the free bubbles. According to the model, all those values are determined by the detachment angle γ_s. These parameters can be used as initial values in the model of bubble transport proposed by Liger-Belair, thus enabling the models of bubble formation and transport to be coupled.

3. Results

A. Simulation of Bubble Formation. For the model simulations, the ambient pressure P_{amb} is set to be 1 bar: although, since this will vary with the depth of the fiber in the fluid, other values are explored below. The initial value of P_t is set at 6 bar, as this corresponds to a concentration of carbon dioxide of

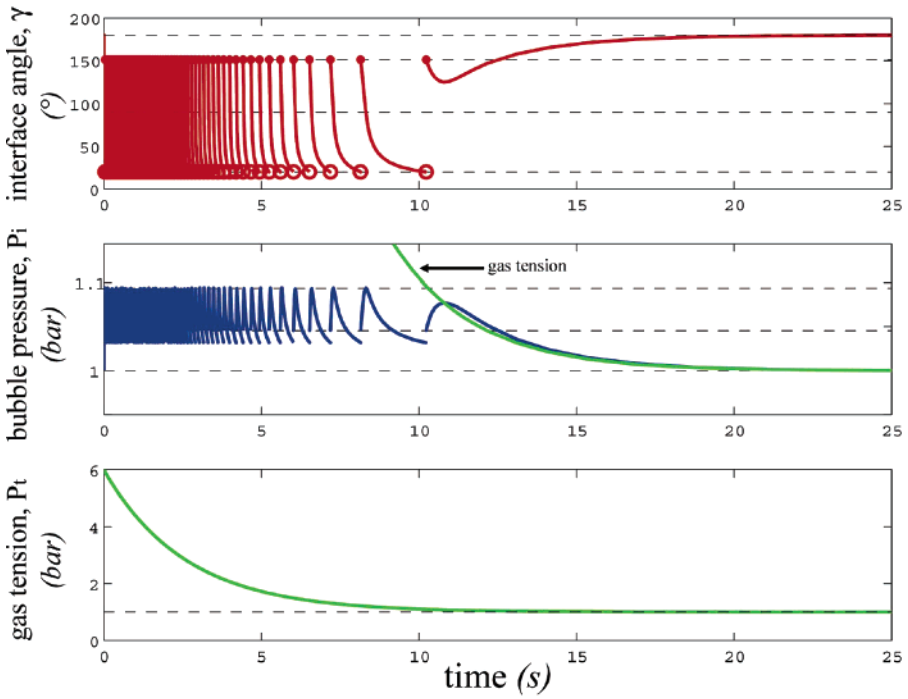

Figure 6. Simulation of the life of a stream for the default values of r, d, and γ_s using the scaled time constant $\{\tau/400\}$.

between 10 and 12 g/L.[3] This is intended to simulate the situation immediately after pouring a glass of champagne. Ambient pressure settles to 1 bar almost immediately whereas the liquid remains supersaturated with CO_2 for a considerable time. We assume that the pressure inside the lumen is initially atmospheric pressure, since the gas trapped in the tubes during the pouring is ambient air. The initial shape of the meniscus is determined by the Laplace equation. The results of this simulation are given in Figure 6, where τ is divided by 400 for illustrative purposes, thus speeding up the process by a factor of 400. The effects of this are examined below.

Once the simulation is launched, carbon dioxide diffuses through the different interfaces, increasing the volume in the bubble and reducing the value of γ. When this reaches its lower value γ_s, a bubble is seeded (this is marked by ○) and the angle is reset to γ_r using the model of detachment. Pressure is also reset to the predicted value of P_3. Note that before this occurs, the pressure passes through a maximum at $\gamma = 90°$, which corresponds to a minimum value of the radius of curvature. It subsequently decreases until a bubble is released, whereupon a new cycle starts. This characteristic style of behavior has been predicted qualitatively;[11] however, here we show that the proposed model is able to capture the quantitative behavior.

The whole time during the process, the difference between the pressure inside the bubble and the gas tension in the liquid (i.e., the driving force) diminishes, which tends to slow the rate of formation. This can be seen in Figure 6 as the time between successive bubbles constantly increases. This continues until $P_t = P_i$, as shown in Figure 6b (the gas tension being plotted as well as the internal pressure). At this point, the driving force reverses and the bubble shrinks. Its top surface goes back to a flat shape since the pressures are finally in equilibrium. The seeding process is thus terminated.

In Figure 7, the solid curve represents the total number of bubbles formed as a function of time. This curve can be very well approximated by an exponential function (dashed): $\tilde{n}(t) = N(1 - e^{-(t/\tau_N)})$. It is not particularly surprising as the rate of variation of γ is proportional to the driving force which decreases exponentially. The formation of a bubble stream can thus be characterized with only two parameters N and τ_N. Indeed, N and τ_N suffice to determine the total number of bubbles seeded and their rate of formation at any time. The effect of the model parameters on these two variables is thus examined in the next section.

It should be noted that all the simulations below have been run for a diffusion time constant τ divided by 100 in order to speed up the processing time. This operation simply scales the final result by dividing N and τ_N by 100. However, this does not affect the initial rate of formation N/τ_N, which remains unchanged. This kind of substitution can be done because the rate of formation of bubbles is much quicker than the diffusion through the top surface of the glass: $\tau_D/\tau \approx 10^{-4}$. Although the exact total number of bubbles formed may be slightly different, this error has been found to be very small.

B. Influence of the Model Parameters. In this section we examine the influence of r, d, and γ_s on bubble formation: the first two because there is found to be significant physical variation in reality, the third because its precise value is difficult to estimate, for the reason outlined earlier. We thus simulate the phenomenon for a range of these parameters. According to what has been observed in a flute of champagne,[4] the radius of the lumen is likely to be a range 5−15 μm and the length of the tube 50−400 μm. Estimating γ_s is much harder, so a relatively wide interval of $\gamma_s \in [5° \; 35°]$ is considered. Five degrees corresponds to a very large volume of detachment: greater volumes and so smaller values of γ_s do not seem to have been observed experimentally.[3,4] To determine the upper value, we consider the geometrical model of detachment. The volume V_1 is a decreasing function of γ_s, and, intuitively, so is V_2. Yet, the curve in Figure 8a showing V_2 in terms of b (the height of the bottom cone) presents a minimum for $b = 35$ μm. This corresponds to an upper limit for γ_s, as shown in Figure 8b.

The effect of the variation of the length of the fiber, d, on the total number of bubbles produced and their rate of formation for different values of the detachment angle is shown in Figure 9 where r is set at its default value. N is a monotonically increasing function of γ_s but shows a strong nonlinear depen-

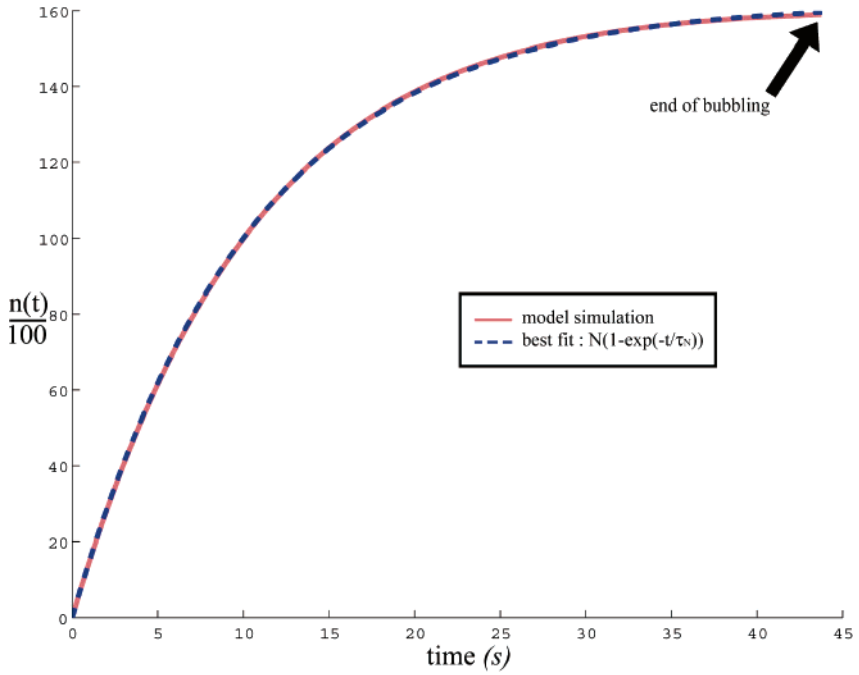

Figure 7. Approximation of the total number of bubbles by $\tilde{n}(t) = N(1 - e^{-(t/\tau_N)})$.

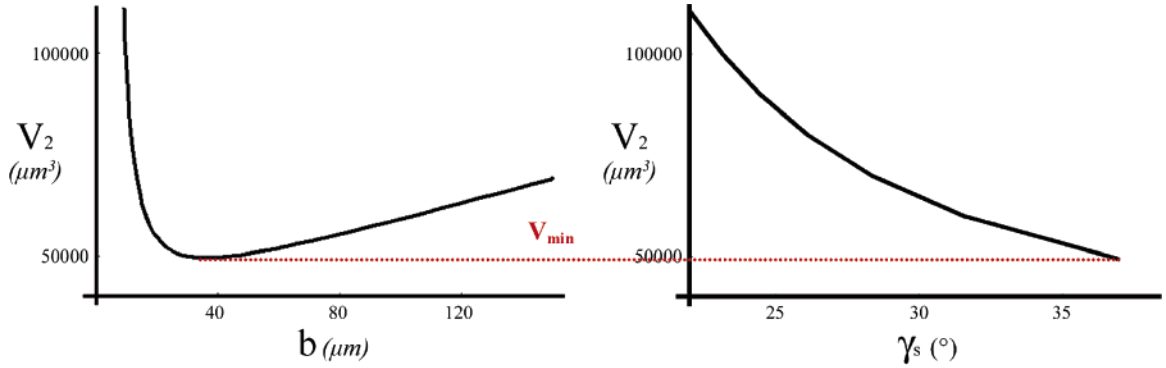

Figure 8. Volume of the bubble at the limit of detachment in terms of (a) b and (b) γ_s.

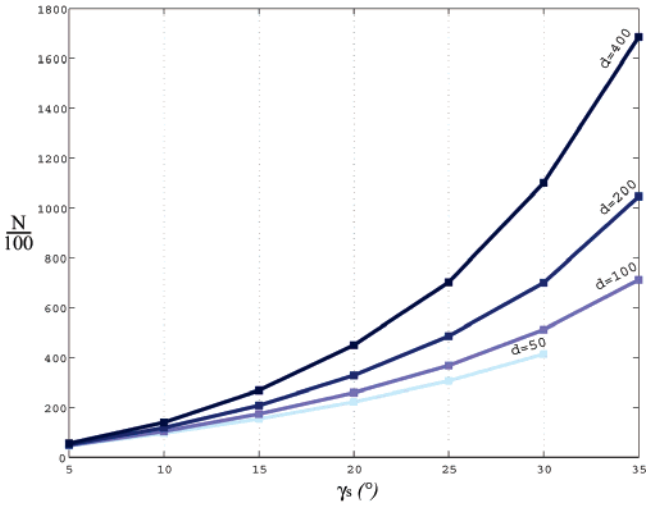

Figure 9. Evolution of the coefficient N for a range of detaching angles and tube lengths (μm).

dence on γ_s. This is because the greater this latter value is, the smaller the released volume and so the shorter time it takes to fill up. In addition, an increase of d (in other words, of the lateral surface area of the lumen) slightly speeds up the phenomenon. Notice that this is a relatively small effect and so the number of bubbles is not strongly dependent upon the lumen length, particularly at small values of detachment angle.

For $d = 50$ μm, the absence of a solution at $\gamma_s = 35°$ is explained by the fact that, according to the geometrical model of detachment, the value of the return angle, γ_r, would be less than 90°, which corresponds to a shape of meniscus that has never been observed in the past.

Figure 10 illustrates in the same manner the influence of r for a lumen with $d = 100$ μm. In this case, and for the same reasons cited before, the narrower the tube, the more bubbles are formed. The influence of this parameter is however considerably stronger.

From all the simulations, it appears that τ_N is entirely conditioned by τ, the time constant for diffusion across the top surface. Its value is found to be constant at 1040 s as any of the other model parameters are varied. This is very similar to τ, as could be expected. The time course of the bubble stream is thus entirely determined by the diffusion time constant at the surface rather than any other parameter.

The influence of other parameters such as the surface tension σ, the time constant τ_D, or the ambient pressure P_{amb} can also be considered, although since these are much more well characterized they are less likely to vary significantly. We have found that N is approximately inversely proportional to τ_D, a relationship which is suggested by eq 13 and the fact that N is

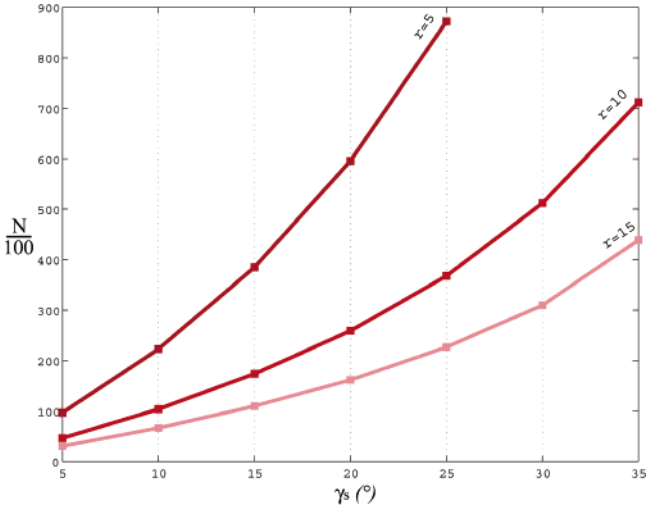

Figure 10. Evolution of the coefficient N for a range of detaching angles and tube radii (μm).

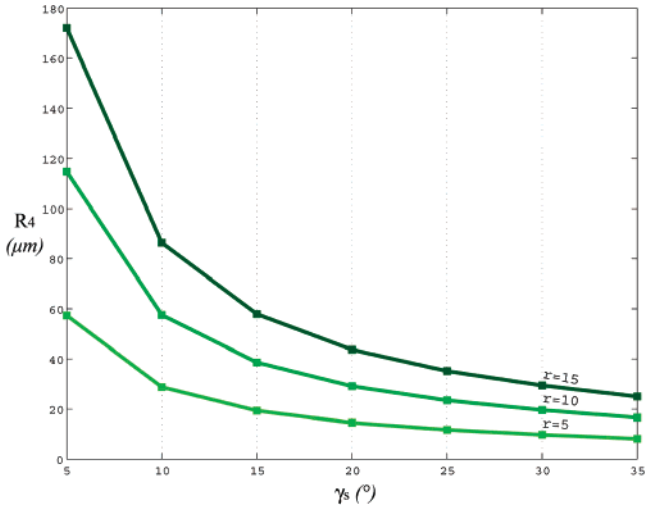

Figure 11. Evolution of the radius of the released bubble for a range of detaching angles and tube radii (μm).

strongly conditioned by dγ/dt, since P_{amb} is constant during the process. A similar ratio is found between N and P_{amb}. Indeed, at the bottom of the flute, where the ambient pressure is 1% greater, N is reduced in the same proportions. However, this is a very small effect and the position of the lumen appears to have very little impact on the model behavior.

Finally, σ does not seem to affect significantly the process. A doubling of its value leads to a diminution in N of only 10%. This appears to be because in eq 13, the term $2\sigma\epsilon \cos \gamma$ is small compared to $(1/4)(r^2/d)P_i \operatorname{cosec}^4(\gamma/2)$.

Concerning the size of the bubbles immediately following detachment, we briefly consider the influence of only two parameters: r and γ_s. Figure 11 illustrates the modifications of the radius R_4, i.e., the initial radius of the detached bubble, for the same range of parameter values as previously. This radius seems to be close to linearly proportional to r and inversely related to γ_s. At small values of detachment angle, the lumen thus produces relatively few but large bubbles.

4. Discussion

From the model results presented here, Figures 9 and 10, it appears that at certain values of γ_s, the initial rate of formation of bubbles (N/τ_N), are much greater than what has been observed experimentally.[3] Indeed, in reality, 25 bubbles/s seems to be the upper limit whereas our simulations lead to greater rates from $\gamma_s \approx 20°$. According to this model, this would mean that some explored values of γ_s are improbable. In addition, a lower limit of the detachment angle can be determined by considering that detachment only occurs because of buoyancy, in other words, when the buoyancy force $F_B = (4/3)\pi R^3 \rho g$ is greater than the capillary force $F_C = 2\pi r\sigma \sin \gamma_s$. This angle is determined by the following equation

$$\sin \gamma_s = \left(\frac{2}{3}\frac{r^2 \rho g}{\sigma}\right)^{1/4} \tag{16}$$

where ρ is the density of the liquid (kg m^{-3}) and g is the acceleration due to gravity (m s^{-2}).

The minimum corresponding value of γ_s (for $r = 5$ μm) is found to be 2.5°. This is clearly an absolute lower limit, which is likely to be far from the actual value, as many other processes also occur, such as suction by the stream. More detailed experimental measurements will be required to determine this angle and to investigate the influence of other bubbles on this parameter. It is likely that in very fast bubble streams this value will be larger (i.e., bubbles detaching will tend to "suck" the succeeding bubble), reducing as the bubble stream slows.

It should be noted here that the rapid change in lumen internal pressure after bubble detachment is an extremely important factor in this process. Although the difference of pressure between P_3 and P_1 is typically only 1%, if this difference is not considered, the model rapidly leads to a completely instable state. This instability generates significant errors after only a few seconds as the error is accumulated each cycle. The two parts of the model thus both play a vital role in modeling both the growth and the detachment of bubbles over the whole lifetime of the process.

Clearly, the model presented here is an idealized one: in reality, the shape of the bubbles as they form and emerge from the fiber may be somewhat different. High-speed photographs[14] seem to indicate that the bubble may not form at the tip under some conditions and that the liquid−gas interface may return inside the fiber after bubble formation, this interface moving toward the fiber tip as gas continues to diffuse. It is suggested here that this is due to the nonideal shape of the end of the fiber and that, in an idealized fiber, the latter process would not occur. In addition, the fibers are photographed in a horizontal orientation and this will affect the movement of gas leading to the formation of the bubble. Although this two-stage process could be simulated in a manner similar to that proposed here, the simplified model presented here is a first step to understanding the processes of bubble formation and directly applies to other situations, where gas is emerging from a cylindrical nucleation site.

5. Conclusions

The model presented in this paper thus enables the formation of bubble streams within carbonated beverages to be simulated easily and quickly, particularly using the time scaling outlined. Bubble formation is found to be promoted in narrow long fibers and to be very sensitive to the value of the detachment angle. For large numbers of bubbles, this detachment angle should be kept as large as possible. The resultant size of these bubbles is found to be very small. Although we have estimated the value of this detachment angle, using buoyancy, and explored its importance on the model behavior, experimental measurements will be valuable in determining its precise value.

The depth of the fiber within the beverage and the surface tension of the bubble in the liquid have only a small impact on the model behavior. However, we have not considered the role of surfactants in the formation of bubbles, which might have an impact on the model.

Finally, we note that this model was originally based on one for the formation of bubbles within crevices in vessel walls in the bloodstream, where bubbles are implicated in decompression sickness, or "the bends". The two models show interesting similarities, but also some marked differences, particularly in the total number of bubbles formed, which is known to be considerably smaller in humans.

Acknowledgment. M.A.C. is supported by the Engineering and Physical Sciences Research Council, U.K.

Appendix A

Justification for the Use of the Steady-State Laplace Equation. The Laplace equation is an approximation of a more general expression, which considers the resistance of the fluid to the motion of the bubble interface. This equation is known as the Rayleigh−Plesset equation[15]

$$\rho R\left(\frac{d^2R}{dt^2} + \frac{3}{2R}\left(\frac{dR}{dt}\right)^2\right) = P_i - P_{amb} - \frac{2\sigma}{R}$$

where ρ is the density of the fluid and is approximately 1000 kg m^{-3}. We have calculated the magnitude of the dynamic terms on the left-hand side of the above equation and found it to be approximately 1 Pa under all the conditions considered in this paper. Since this is completely negligible in comparison to the values of pressures inside and outside the bubble, the dynamic terms can safely be neglected, even when the bubble streams are at their fastest.

References and Notes

(1) Lubetkin, S. D.; Blackwell, M. The nucleation of bubbles in supersaturated solutions. *J. Colloid Interface Sci*. **1988**, *26*, 610.

(2) Jones, S. F.; Evans, G. M.; Galvin, K. P. Bubble nucleation from gas cavities—a review. *Adv. Colloid Interface Sci.* **1999**, *80*, 27−50.

(3) Liger-Belair, G.; Vignes-Adler, M.; Voisin, C.; Robillard, B.; Jeandet, P. Kinetics of gas discharging in a glass of champagne: The role of nucleation sites. *Langmuir* **2002**, *18*, 1294.

(4) Liger-Belair, G.; Voisin, C.; Jeandet, P. Modeling nonclassical heterogeneous bubble nucleation from cellulose fibers: Application to bubbling in carbonated beverages. *J. Phys. Chem. B* **2005**, *109*, 14573−14580.

(5) Chappell, M. A.; Payne, S. J. A physiological model of gas pockets in crevices and their behavior under compression. *Respir. Physiol. Neurobiol.*, in press.

(6) Srinivasan, R. S.; Gerth, W. A.; Powell, M. R. Mathematical models of diffusion-limited gas bubble dynamics in tissue. *J. Appl. Physiol*. **1999**, *86*, 732−741.

(7) Lango, T.; Morland, T.; Brubakk, A. O. Diffusion coefficients and solubility coefficients for gases in biological fluids and tissues: a review. *Undersea Hyperbaric Med.* **1996**, *23*, 247−272.

(8) Liger-Belair, G.; Topgaard, D.; Voisin, C.; Jeandet, P. Is the wall of a cellulose fiber saturated with liquid whether or not permeable with CO_2 dissolved molecules? Application to bubble nucleation in champagne wines. *Langmuir* **2004**, *20*, 4132−4138.

(9) Liger-Belair, G. *Uncorked*: *The Science of Champagne*; Princeton University Press: Princeton, NJ, 2004.

(10) Atchley, A. A.; Prosperetti, A. The crevice model of bubble nucleation. *J. Acoust. Soc. Am.* **1989**, *86*, 1065−1084.

(11) Liger-Belair, G. *Ann. Phys. Fr.* **2002**, *27*, 1.

(12) Manasseh, R.; LaFontaine, R. F.; Davy, J.; Shepherd, I. C.; Zhu, Y. Passive acoustic bubble sizing in sparged systems. *Exp. Fluids* **2001**, *30* (6), 672−682.

(13) Liger-Belair, G.; Prost, E.; Parmentier, M.; Jeandet, P.; Nuzillard, J.-M. Diffusion Coefficient of CO_2 Molecules as Determined by ^{13}C NMR in Various Carbonated Beverages. *J. Agric. Food Chem*. **2003**, *51*, 7560.

(14) Liger-Belair, G.; Tufaile, A.; Robillard, B.; Jeandet, P.; Sartorelli, J. C. Period-adding route in sparkling bubbles. *Phys. Rev. E* **2005**, *72*, 037204.

(15) Eller, A.; Flynn, H. G. Rectified diffusion during nonlinear pulsations of cavitation bubbles. *J. Acoust. Soc. Am.* **1965**, *37*, 493−503.